Production of Ni-35Ti-15Hf alloy via the FFC Cambridge Process

B. X. Wang[a, b, z], R. Bhagat[b], X. Z. Lan[a] and R. J. Dashwood[b]

[a] School of Metallurgical Engineering, Xi'an University of Architecture and Technology, Xi'an 710055, P. R. China

[b] Warwick Manufacturing Group, University of Warwick, Coventry CV4 7AL, United Kingdom

[z] E-mail: wwangbixia@hotmail.com

Tel:+86-029-82205147

Fax:+86-029-82205083

Abstract

The NiTiHf system alloy is considered to be one of the most attractive shape memory alloy (SMA) at elevated temperatures. This paper outlines how the FFC Cambridge Process was applied to produce the Ni-35 at.% Ti-15 at.% Hf (henceforth referred to as NiTiHf) alloy from sintered precursors of NiO, TiO_2 and HfO_2. In order to illuminate the reduction pathway, a number of partial reductions were completed at different reduction times. The samples were characterised by SEM, X-EDS and XRD. It was found that the key stages of reduction involved：(1) the reduction of $NiTiO_3$ and NiO to Ni, (2) the reduction of $CaTiO_3$ to Ti and the simultaneous formation of Ni_3Ti, (3) the reaction of Ni_3Ti with $CaTiO_3$ to form NiTi, (4) the reduction of HfO_2 and $CaHfO_3$ to form NiTiHf alloy and finally (5) the deoxidation and the Ti/Hf homogenisation of NiTiHf alloy. The sintered oxides precursors were reduced to metal alloy after nine hours reduction. After twenty-four hours reduction, a homogeneous alloy was formed with an oxygen content of 1600 ppm. DSC analysis shows that the austenite transformation temperature of the produced NiTiHf alloy was close to that seen in literature. An electrochemical predominance diagram for the Hf-Ca-Cl-O system was constructed to help understand the reactions during reduction.

Key words

Shape memory alloys; NiTiHf; Electro-deoxidation; Molten salt

Introduction

Binary NiTi alloys have a long history of use as superelastic and shape memory components [1]. In the early 1960s, Buehler *et al.* [2] discovered the shape memory effect in an equiatomic alloy of nickel and titanium. Since then, intensive investigations have been made to elucidate its mechanical properties and to exploit its potential applications. Currently NiTi is being used in a number of applications from actuators in the aerospace sector to damage-resistant frames for eyeglasses to use in biomedical implants [3].

The austenite transformation temperature of NiTi alloys is below 100°C, which has limited their utility for the many technological applications requiring higher operating temperatures [4,5]. Ternary NiTi blended with Hf, Zr, Pd or Pt additions to increase the austenite transformation temperatures have been studied [6,7]. Currently, Hf addition is considered to be the most attractive option due to improved thermal stability and lower cost of producing NiTiHf alloys as compared with NiTi-Pd and NiTi-Pt alloys [5]. It has been shown that Hf additions elicit a positive response in NiTi as demonstrated by Wojcik [1] and Meng *et al.*[8]: Hf additions can enhance the austenite transition temperature with 10 at. % Hf resulting in austenite temperature almost 100°C higher than conventional Ni-Ti alloys.

NiTiHf alloys are conventionally produced by vacuum arc melting pure Ni, Ti and Hf metals and casting into water cooled copper molds. In order to get a homogeneous sample the melting and re-melting process need to be repeated at least five to six times in an argon atmosphere [9]. Also, it was found that the NiTiHf alloys without further thermo-mechanical treatments to homogenise and refine the grain structure suffer from poor fabricability and deficient mechanical properties [4].

The FFC Cambridge process [10] is a direct electrochemical method to form metal from metal oxide using a molten salt. The process has been demonstrated for Ti based alloys such as Fe-Ti [11], Ni-Ti [3,12], Ti-W[13] and Ti-Mo[14].The preparation of NiTi alloy from

mixed TiO_2 and NiO, which was first proposed by Zhu *et al.* [12] was then systematically investigated by Jackson *et al*. [3].

This paper will demonstrate the production of NiTiHf alloy via the FFC Cambridge process by using NiO, TiO_2 and HfO_2 as starting materials. The reduction pathway of the oxides to metal alloy will be presented using a series of partial reductions. It is envisaged that the FFC Cambridge process will enable the low-cost production of homogenous NiTiHf, when compared with the conventional method. This will be achieved by using lower cost starting materials; the process is a solid state process thus removing costly melting stages.

Experimental

The precursors were formed using reagent grade TiO_2 (99.5%，-325mesh, Alpha Aesar), NiO (99%, -325mesh, Alpha Aesar) and HfO_2 (99%, -325mesh, Alpha Aesar) were ball-milled together with methanol and zirconia spheres for 24 h. The slurry was then dried and the powder ground in a mortar and pestle with small quantities of distilled water, which acted as a binder for the initial stages of pellet production. One gram of the powder was placed in a 13 mm diameter die and subjected to a uniaxial compressive pressure of 111 MPa for 60s. The compacted pellet was then drilled by hand with a 3 mm diameter TiN drill piece. The oxide pellets were placed on an alumina firing trough and into a furnace. The precursors were heated at a rate of $3°C \cdot min^{-1}$ and sintered in air at 1100°C for 2 hrs and then furnace cooled.

A schematic of the electrochemical cell used in all the reduction experiments is shown in Fig. 1. The reduction cell is constructed from Inconel® with a water-cooled stainless steel top plate (SFL Instron). The cell is housed in a vertical programmable tube furnace (SFL Instron). The molten Calcium Chloride ($CaCl_2$) salt was contained in a grade 2 CP-Ti crucible with an outer diameter of 90 mm, a wall thickness of 10 mm, and a height of 200 mm.

Dehydrated $CaCl_2$ granules (99.7%, Fluka Analytical) were contained in a CP-Ti crucible and thermally equilibrated at 100°C for 3 hrs, then heated to 300°C at a rate of 0.1°C·min^{-1}. The $CaCl_2$ was then heated to 900°C at 3°C·min^{-1}, under argon (BOC pureshield, -200 mL·min-1) and equilibrated for 30 mins before electrolysis starts.

The sintered oxides precursor was attached to the CP-Ti current collector and slowly lowered into the molten $CaCl_2$ salt. The pellet was polarized from OCV to -3.2 V vs carbon anode at a rate of 0.01 V·s^{-1}. Samples were reduced for the periods of 10 mins, 1, 3, 5, 9, 17 and 24 hrs respectively.

Following reduction, samples were washed for 30 mins in an ultrasonic bath to remove residual salt and prepared for analysis using standard metallographic techniques. The samples were characterised using X-ray energy-dispersive spectroscopy (X-EDS), secondary electron imaging (SEI) and backscattered electron imaging (BEI) using a field emission gun scanning electron microscope (FEG-SEM) (Carl, Zeiss).

All samples were characterised using X-ray diffraction (XRD) with a Phillips PW 1710 diffractometer. If the sample was mostly ceramic, it was ground to a fine powder for analysis; if the sample was partially metallic, it was ground on one surface to its core (using 800 grit SiC paper) to reveal different layers for XRD analysis. Phases were identified by using information obtained from the Chemical Database Services.

The oxygen content of 24 hrs reduced sample was determined using a Eltra ON – 900 Oxygen/Nitrogen Determinator. DSC testing was conducted on this sample using Mettler Toledo DSC 1, applying an aluminum standard and a temperature ramp rate of 10°C·min^{-1}.

Results and Discussion

The electrochemical reduction of metal oxides in $CaCl_2$ can be described by constructing electrochemical predominance diagrams described by Dring *et al*. [15]. In this study, the

predominance diagram for the Hf-Ca-O-Cl system was calculated，then it was overlaid with the Ni-O-Ca-Ti-Cl diagram [3] and shown in Fig. 2. Due to the absence of thermodynamic data for $HfCl_2O$ and $HfOCl_2$, they were not included in this diagram. The combination of these two diagrams predicts the following electrochemical reduction pathways; (1) Ni will first form from NiO and $NiTiO_3$, (2) the Ni will react with $CaTiO_3$ to form Ni_3Ti, (3) the Ni_3Ti will react with $CaTiO_3$ to form NiTi and finally when Hf is reduced from $CaHfO_3$ and HfO_2, it forms a solid solution with NiTi to produce the NiTiHf alloy.

Ruh *et al.* [16] investigated the phase relations in the HfO_2-TiO_2 system. Krebs *et al*. [17] studied various crystalline mixtures in HfO_2-TiO_2 systems and concluded that the equilibrium conditions for the formation of $HfTiO_4$ were not achieved in HfO_2-TiO_2 mixtures until the firing temperature exceeded 1300°C. As a sintering temperature of 1100°C was employed in this study $HfTiO_4$ should not be present. XRD (Fig. 3a) and SEM (Fig. 4a) analysis shows that when powders of NiO, TiO_2 and HfO_2 were mixed and sintered at 1100°C for 2h, $NiTiO_3$ was formed with large quantities of HfO_2 remaining unreacted. Even if the sintering temperature were increased to 1300°C, the more thermodynamically favourable reaction to form $NiTiO_3$ (ΔG=-770 kJ at 1300°C) will consume all of the TiO_2. It can be seen from the BEI (Fig. 4a) that large amounts of $NiTiO_3$ appear in the as sintered precursor. Unreacted particles of NiO can be observed, most likely resulting from the agglomeration of smaller NiO particles at high temperature. The HfO_2 powders are bi-modal with some particles scattered in the $NiTiO_3$ phase and others gathered on the surface of ~2μm particles.

The XRD trace (Fig. 3b) of the 10 mins reduction sample reveals the presence of Ni, $CaTiO_3$ and $Ca(Ti,Hf)O_3$.The absence of $NiTiO_3$ and NiO species, indicates that after 10 mins reduction, Ni was formed from $NiTiO_3$ and NiO via Reactions (1) and (2). It has been observed by Jackson *et al.* [3] that $NiTiO_3$ forms Ni and $CaTiO_3$ when soaked in the molten salt for 600s with no applied potential and they think it may be due to the creation of galvanic cell between the Ti current collector and the NiO in the pellet precursor. When the NiO and

the Ti are placed in contact with each other, the Ti will preferentially oxidize to TiO_2 and the NiO will be reduced to Ni.

$$NiTiO_3 + 2e^- = TiO_2 + Ni + O^{2-} \quad (1) \quad E^0_{1173K} = -0.88V$$

$$NiO + 2e^- = Ni + O^{2-} \quad (2) \quad E^0_{1173K} = -1.519V$$

The standard Gibbs free energy formation of NiO at 1173K (-133.576 KJ/mol) is higher than that of TiO_2 and HfO_2 (-732.128 KJ/mol and -901.734 KJ/mol respectively at 1173K), thus NiO is the phase easiest to be reduced.

It can be seen from BEIs (Fig. 4b) that Ni particles are formed in the pores of the pellet, at the same time large quantities of $CaTiO_3$ are generated, surrounding the Ni particles. A solid solution of $CaTiO_3$ and $HfTiO_3$ (Fig. 4b) was detected by X-EDS within the pellet and will be referred to as $Ca(Ti,Hf)O_3$. The ratio of Ca:Ti:Hf:O was determined to be 23:13:10:54, respectively. In the XRD trace of the sample, the peaks of $CaHfO_3$ are shifted, which is likely to be caused by the presence of titanium in solid solution. The shifted peaks was marked as $Ca(Ti,Hf)O_3$ in Fig. 3. It was observed that $Ca(Ti,Hf)O_3$ appears in the vicinity of the $CaTiO_3$ particles (Fig. 4b).

The presence of $CaTiO_3$ and $HfTiO_3$ in Fig. 4b corresponds well with the presence of Ni particles. This is most likely because the rapid reduction of $NiTiO_3$ and NiO results in the release of a large quantity of oxide ions into the electrolyte, which results in a significant decrease in the local pO^{2-} of the electrolyte. This would results in a shift to the left side of the electrochemical predominance diagram (Fig. 2), which would increase the likelihood of the chemical formation of $CaTiO_3$ and $HfTiO_3$ through Reactions (3) and (4). The formation of Ni particle and the presence of $CaTiO_3$ and $HfTiO_3$ are the first stage of the electrochemical reduction of mixed metal oxides to NiTiHf alloy.

$$TiO_2 + Ca^{2+} + O^{2-} = CaTiO_3 \quad (3) \quad \Delta G^0_{1173K} = -759.11 KJ/mol$$

$$HfO_2 + Ca^{2+} + O^{2-} = CaHfO_3 \quad (4) \quad \Delta G^0_{1173K} = -765.9 KJ/mol$$

After 1 h of reduction, three layers (Fig. 5b) can be observed in the cross section of the samples. The XRD analysis shows the appearance of two phases in addition to the phases observed in 10 mins sample: NiTiHf alloy in the edge layer and Ni_3Ti in the core of the sample. The appearance of Ni_3Ti marks the second stage of the reduction process.

The thickness of the edge layer (Fig.s 4c and 5b) is approximately 100 μm, which is composed of an inhomogeneous NiTiHf alloy, with the particle size less than 10 μm. X-EDS analysis reveals a composition of 51 at. % Ni, 32 at. % Ti and 17 at. % Hf. No oxygen was detected by X-EDS, X-EDS shows the middle layer (Fig. 4d) is also an alloy, with a smaller particle size (less than 4 μm) and a higher oxygen content (8-18 at. %).

The presence of Ni_3Ti is observed in the BEI (Fig. 4e) of the core layer, which is accompanied by the formation of $Ca(Ti,Hf)O_3$. As the electrochemical reduction progressed, $CaTiO_3$ was reduced to Ti, which simultaneously reacted with Ni to form Ni_3Ti via Reaction (5). As a consequence, oxide ions are released into the electrolyte, resulting in the formation of $Ca(Ti, Hf)O_3$. X-EDS analysis indicates that the $Ca(Ti,Hf)O_3$ solid solution has a wide range of compositions, with the ratio of Ti:Hf ranging from 14:4 to 11:13. The phase with the former ratio appears darker in the BEI. Ni particles and large quantities of HfO_2 particles are also observed in the core layer.

$$3Ni + CaTiO_3 + 4e^- = Ni_3Ti + Ca^{2+} + 3O^{2-} \qquad (5) \qquad E^0_{1173K} = -2.78V$$

The XRD patterns of 1 h core layer reveal the presence of NiTiHf, however this does not mean that the alloy formed in the core of the sample. This is because the cylindrical surface of the reduced pellet is also alloy and can't be removed when expose the core layer of the sample for XRD analysis by grinding. The same situation occurred in the XRD traces of the core layer of the 3 h and 5 h sample.

In order to study the homogeneity of the NiTiHf alloy formed in the edge layer of the 1 h sample, elements map were collected by X-EDS and are shown in Fig. 6. It was found that Ni

is uniformly distributed throughout the sample, whilst the distribution of Ti and Hf elements varies. Ti rich material appears to be located in the center of the alloy particles whilst Hf rich material occurs on the edge of the particles. The observed distribution of elements, at the early stage of reduction results from the segmented reduction sequence of the metal oxides present. As a majority of the Hf is was present as large particles it stands to reason that Hf homogenisation will begin by enriching the outside of NiTi particles. Therefore it can be conclude that homogenization of Hf at this stage of reduction is not complete. A more finely distributed HfO_2 powder would mitigate this inhomogeneity issue.

It can be seen in the BEI (Fig. 5c) that after 3 h of reduction, the layered structure has further developed with the edge layer increasing in thickness to approximately 300 μm. In addition the outer layer appears to be more porous than the inner layers. No additional phases were detected by XRD analysis. The Ni particles previously observed in the 1 h sample are now fully transformed to Ni_3Ti by reaction (5).

The BEI (Fig. 4f) and X-EDS of the edge layer shows the presence of NiTiHf alloy with a particles size of less than 10 μm. It is observed that the middle layer (Fig. 4g) is composed of small particles of NiTiHf alloy, with a size of 2-4 μm. The X-EDS analysis reveals an oxygen content of 0-12 at.%, which indicates the NiTiHf alloy forms with oxygen in solid solution. However, the alloy particles with lower oxygen content are inhomogeneous.

It can be observed that after 3 h of reduction more Ni_3Ti and $Ca(Ti,Hf)O_3$ appear in the core layer of 3 h sample (Fig. 4h). The X-EDS analysis shows that the $Ca(Ti, Hf)O_3$ phase has a range of composition. Significantly more $Ca(Ti, Hf)O_3$ was detected than observed in the 1 h sample.

It can be seen from Fig. 5d that after 5 h of reduction, a majority of the pellet has been electrochemically reduced to metal alloy, with the exception of a small area within the core. The XRD trace of the 5 h reduction sample (Fig. 3g) shows that the main phase in the edge

layer is NiTiHf alloy. It is observed in the BEI (Fig. 4i) that the particle size is less than 15 μm. The X-EDS analysis reveals the NiTiHf particles have a composition of 50 at.% Ni, 33 at.% Ti and 17 at.% Hf, though the Hf content varies.

X-EDS analysis in the middle layer of the sample (Fig. 4j) shows that it is primarily composed of NiTiHf alloy, with an average oxygen content of 10 at.%, with particles showing a Hf inhomogenity. An average particle size of ~6 μm was observed in the BEI (Fig. 3j).

The XRD trace (Fig. 3h) reveals two new phases in the core of the sample, i.e. NiTi and $Ca(Ti,Hf)_2O_4$. The first appearance of NiTi was also observed by Jackson *et. al* [3] in the 6 h reduction sample and it was thought to be formed by the reaction between Ni_3Ti and $CaTiO_3$ (reaction (6)). As can be seen in the predominance diagram, the formation of NiTi by consuming Ni_3Ti and $CaTiO_3$ indicates the third stage of the electro reduction process. However, Ni_3Ti was still the prevailing phase within the core of the sample (Fig. 7). Firstly because NiTi has a narrow homogeneity range, and secondly the Ni_3Ti observed in this ex-situ study is believed to precipitate upon cooling due to the reduction of Ni solubility in NiTi at lower temperatures [3].

$$Ni_3Ti + 2CaTiO_3 + 8e^- = 3NiTi + 2Ca^{2+} + 6O^{2-} \qquad (6) \quad E^0_{1173K} = -3.00V$$

As discussed before, the peaks of $CaTi_2O_4$ appear to be shifted in the XRD traces, which is likely due to the presence of Hf in solid solution with $CaTi_2O_4$, which will henceforth be referred to as $Ca(Ti,Hf)_2O_4$. Calcium di-titanate ($CaTi_2O_4$) was also reported in the works of Schwandt *et al.* [18] and Bhagat *et al.* [19]. Bhagat *et al.* [19] concluded that the phase was formed from the comproportionation of TiO and $CaTiO_3$, whilst in the presence of Ti. Fig. 7 shows small particles of NiTi gathered embedded together within the bulk of $Ca(Ti, Hf)O_3$ and $Ca(Ti, Hf)_2O_4$. However, in the core layer Ni_3Ti was observed as discrete particles.

In the BEIs (Fig. 7), the phase $Ca(Ti,Hf)_2O_4$ appears brighter when more Hf is present in solid solution. This can be seen in Fig.7, where the solid solution $Ca(Ti,Hf)_2O_4$ with 14 at.% Ca, 18 at.% Ti and 10 at.% Hf appears to be brighter than a mixture of $Ca(Ti,Hf)_2O_4$/ NiTi (12 at.% Ca, 28 at.% Ti, 10 at.% Ni, 6 at.% Hf and 44 at.% O).

No distinct layers were observed in the cross section of 9 h reduced sample (Fig. 5e). The edge part of the pellet does appear to be less dense than the core. BEI and X-EDS of the edge layer (Fig. 8a) shows the particle size of the NiTiHf alloy is approximately less than 20 μm. The edge layer was found to be Hf rich, with the average composition of 50 at. % Ni, 30 at. % Ti and 20 at. % Hf. It can be observed in the XRD trace (Fig. 3i) of this layer that some peaks of the NiTiHf alloy are less intense than that of the 24 h sample.

The XRD traces of the core layer shown in Fig. 3j demonstrates the presence of NiTiHf and the disappearance of other phases observed in 5 h sample, which indicates that the entire pellet was reduced to NiTiHf alloy. Some peaks were found to be wider and less intense, which is likely due to an inhomogeneity of the alloy. X-EDS of the core layer (Fig. 8b) confirms this as a significant difference in element composition was detected, i. e., 42-50 at. % Ni, 32-49 at. % Ti and 9-19 at. % Hf.

No oxygen content was detected by X-EDS within the pellet, however it is thought that there is a quantity of oxygen below limits of detection of the equipment used.

The predominance diagram (Fig. 2) shows that the reduction of HfO_2 to Hf and $CaHfO_3$ to Hf occur at increasingly negative potentials, i. e. -2200mv for HfO_2 reduction at pO^{2-}=8, and –3000mv for $CaHfO_3$ reduction at pO^{2-} = 3, which suggests that the formation of Hf and then the alloy of NiTiHf through Reactions (7)-(8) will be the fourth stage of the reduction process.

$$NiTi + HfO_2 + 4e^- = NiTiHf + 2O^{2-} \quad (7)$$

$$NiTi + CaHfO_3 + 4e^- = NiTiHf + Ca^{2+} + 3O^{2-} \quad (8)$$

After 9 h reaction, the sintered NiO, TiO_2 and HfO_2 oxides pellet was found to be fully reduced to NiTiHf alloy. Jackson *et al.* [20] reduced NiO and TiO_2 to NiTi in 12 h, a full 3 hrs more than was observed in this work. Jackson *et al.* [20] observed consolidated outer metal alloy layers in partially reduced samples, which was attributed to sintering during the reduction process. Thus the regions that form metal initially will have a greater degree of sintering. As it has been confirmed that electroreduction of a solid oxide proceeds through the propagation of the metal-oxide-electrolyte three-phase interlines (3PIs), starting from the surface and then entering the oxide precursor [21,22], the formation of consolidated metal layers on the edge of the samples restricts the penetration of salt into the pellet, which makes the diffusion of oxygen through the electrolyte in the pores of the metal alloy more difficult. However, in this study, the outer metal layers (NiTiHf alloy) were found to be porous. As Hf is a high melting point metal, relative to Ni and Ti, it is thought that its presence in solution with NiTi alloy will restrict the sintering behavior of the NiTi alloy. Reducing the sintering behavior of the metal alloy layer allows greater salt penetration into the pellet, enhancing reduction and deoxidation over pure NiTiHf.

The cross section of the 17 h reduced sample (Fig. 5f) appears more uniform than that observed for the 9 h sample. The only exception is the porous structure observed in the surface layer (~100μm) shown in Fig. 5f. Fig. 8c shows a high magnification BEI of this surface layer. The alloy particles appear to be larger and more interconnected but less elongated. X-EDS reveals the average composition of the alloy is 48-50 at. % Ni, 32-33 at. % Ti and 17-20 at. % Hf, with the Hf content being higher than in the middle layer of the pellet (49-50 at.% Ni, 34 at.% Ti and 16 at.% Hf).

The XRD trace (Fig.s 3k and 3l) show that new peaks appear in addition to those of NiTiHf. They appear to be more intense in the core layer of the sample. It was concluded that these peaks correspond to the Ti rich phase seen in Fig. 8d. The composition of the Ti-rich

phase (Fig. 8d) was found to be 35-37 at. % Ni, 51-53 at. % Ti and 12 at. % Hf. The Ti rich phase accounts for approximately 2% of the core layer.

When the $NiTiO_3$ was reduced to Ni element, TiO_2 was produced simultaneously (reaction (1)). Although most of the TiO_2 goes to form $CaTiO_3$ as shown in reaction (3), a small quantity is able to dissolve into the salt. As Ti has a limited solubility in $CaCl_2$, when the salt is polarized to sufficiently negative potentials, the Ti will come out and deposit on the alloy[20], producing the Ti-rich phase. The deposition of Ti from the salt could be a plausible explanation to the titanium enrichment observed near pores (Fig. 8d).

Similar to 9 h of reduction, no oxygen was detected by X-EDS, however, it is believed a quantity of oxygen still remains in the alloy and will be removed by further reduction. Due to the slow rates of solid state diffusion, additional reduction time is required to produce a homogeneous alloy. This additional reduction time was deemed to be the final stage of electrochemical reduction process. As further deoxidation occurs, homogenisation can take place by the diffusion of atoms.

After 24 hours reduction, it can be observed (Fig. 5g) that the 50µm surface layer of the sample is more porous than the middle layer. BEIs of the sample (Fig.s 8e and 8f) show a porous structure throughout the pellet, with the NiTiHf particles in the middle and core layer being approximately 20µm, bigger than those observed in the surface layer.

After 24 h reduction, the product was determined to be Ni-37Ti-14Hf (atomic %) based on X-EDS analysis. The oxygen content of the material was measured to be 1600ppm using oxygen analysis. When analysing the XRD traces (Fig.s 3m and 3n) of this sample, patterns corresponding to Ni-38Ti-12Hf (atomic %) and Ni-32Ti-18Hf (atomic %) were used to identify the peaks. The homogeneity of Ni, Ti and Hf in the 24 h reduction sample was analysed using X-EDS area scans. The analysis was shown in Fig. 9, indicating that the three elements are homogenously distributed along the cross section of the pellet.

As a summary, the intermediate products and products before and after electrolysis were listed in Table 1.

The current-time plot for the 24 h reduction was shown in Fig. 10. The three-phase interline model [21,22] can be applied to explain the current changes. It can be seen from Fig. 10(b) that when the electrolysis process started, the potential in the cathode reached -3.2V vs carbon anode after 5.5 mins, the current increased sharply to a peak value of 3733mA after 7.5 mins (Point A), indicating a fast reaction speed in the interface of the current collector, the oxides and the molten salt. This may correspond to the first stage of the electro reduction of the mixed NiO, TiO_2 and HfO_2 according to the above analysis of the partially reduced pellet, showing the formation of Ni and $CaTiO_3$. Then the current dropped quickly from 7.5 mins to 22 mins of the electrolysis and three inflexions can be observed during this period of time: the first one was in 14mins (Point B), with the current about 3000mA; the second one was in 17mins (Point C), with the current about 2570mA; and the last one was in 22mins (Point D), with the current about 1800mA. The above inflexions may indicate that different phases i. e. Ni_3Ti, NiTi, and NiTiHf respectively formed in the surface layer of the pellet.

When the surface layer of the sintered pellet was reduced to alloy, the reduction will develop into the pellet, and the oxygen ions produced will diffuse through the salt in the porous of the alloy into the bulk salt. Therefore the reaction speed started to slow down, as shown in Fig. 10a, the current decreased from 1800mA (point D, 22mins) to 1380mA (point E, 53mins),.and then gradually decreased to 750mA until the end of the reaction (point F, 24hrs). It was observed that the slope of curve DE is smaller than curve CD but larger than that of curve EF, this may indicate that under the surface layer, an inner layer of alloy was formed from 22mins to 53mins of reduction based on the above analysis of the 1h partially reduced pellet. After that, the reduction was developed at a relatively steady speed.

The energy consumption data for the NiTiHf preparation is about 40KWh per Kg NiTiHf alloy, which is a very large value due to the long time (24 h) of electrolysis. Li. *et. al.* [21] have found that by increasing the porosity of the TiO_2 precursor, the overall rate of O removal from the oxide increased, which results in the increase of current efficiency and decrease of energy consumption for electroreduction of TiO_2 to Ti. The oxide precursor with higher porosity can be obtained by using a fugitive agent, for example graphite, polymer powder or NH_4HCO_3 [21], which can be burnt out from the precursor during sintering in air at elevated temperatures, with the last one being recyclable, cheap and effective. In order to lower the energy consumption for preparation of the NiTiHf alloy, further work on enlarging the porosity of the mixed oxides pellet needed to be carried out in the future.

DSC testing was conducted on the 24 h reduced sample to determine its shape memory properties with the hysteresis shown in Fig. 11. The hysteresis shows a well-defined single peak, with a smooth initiation of the transformation. The austenitic start temperature (A_s), austenitic finish temperature (A_f), martensitic finish temperature (M_f) and martensitic start temperature (M_s) of the Ni-35Ti-15Hf alloy in this work and that reported by Meng *et al.* [8] for the $Ti_{36}Ni_{49}Hf_{15}$ alloy was shown in Table 2.

It can be seen from Table 2 that the A_f and M_s values of the alloy in this work are close to that from Meng *et al.* [8], while A_s and M_f are lower. This is possibly due to the inhomogeneity in oxygen content and the higher oxygen content (1600ppm) of the Ni-35Ti-15Hf alloy. It was found by Wojcik [1] that the NiTiHf alloy with lower oxygen content has a higher transition temperature. Although the oxygen content of the $Ti_{36}Ni_{49}Hf_{15}$ alloy was not mentioned in Meng's work, it was thought that the value should be close to 330 ppm determined by Wojcik [1], as the alloys were made by similar method.

In addition, the transformations peaks are broader than those observed by Meng *et al.* [8] and are most likely due to micro segregation effects. This is evidenced by the fact that the transformation peaks become increasingly narrow with additional DSC heating cycles, which

further homogenise the alloy. An inhomogeneous oxygen content in the alloy could also elicit a similar response and broadens the peaks

TiC was observed by Rohit *et al.* [14, 19] on the surface of the pellets (Ti and Ti-Mo alloy) during the later stage of reduction, and its formation mechanism was thought to be the chemical reaction of Ti with C. However, no TiC was observed during this work, which is consistent with the work of Jackson *et al*. [3]. It is thought that this is indicative of the Ni-Ti system and that the Ni-Ti-Hf system is similar.

Conclusions

This study demonstrates the ease of producing Ni-35Ti-15Hf alloy via the FFC Cambridge Process. After 9 hours reduction, the sintered metal oxides pellet was fully reduced to NiTiHf alloy with a quantity of oxygen in solid solution. HfO_2 additions were found to improve the reduction kinetics leading to a more rapid reduction than that observed for pure NiO and TiO_2 mixes to form NiTi [3].It was concluded that the presence of high melting point Hf retards the sintering of NiTi. Thus when metal layers are formed in the sample they remain sufficiently porous to allow good molten salt penetrating whilst keeping the oxygen diffusion distances relatively small. This results in an accelerated reduction process over that observed for pure NiTi formed via FFC Cambridge process.

The 24 h reduced product was found to be a homogeneous NiTiHf alloy, with an oxygen content of 1600ppm. The transformation temperatures of the alloy determined by the DSC test are close to that in the work of Meng *et al*. [8], indicating a high temperature shape memory alloy with the austenite peak of 216°C. Whilst the transformations peaks are broader due to micro segregation effects and inhomogeneity of oxygen content in the alloy.

The electrochemical reduction process of NiTiHf alloy can be divided into five distinct stages (a-e):

(a) The first stage was the reduction of elemental Ni from $NiTiO_3$ and NiO. This phenomenon was discovered to occur initially at open circuit and at a greater degree after 10 mins reduction. $CaTiO_3$ and $Ca(Ti,Hf)O_3$ were observed to form in the first stage, most likely a result of TiO_2 absorbing oxide released from the reduction to form Ni.

(b) The second stage of the process is the reduction of $CaTiO_3$ to form Ti and the subsequent reaction with elemental Ni to form Ni_3Ti.

(c) The third stage of the process was the formation of NiTi by consuming Ni_3Ti and $CaTiO_3$.

(d) The fourth stage of the process was observed to be the reduction of HfO_2 and $CaHfO_3$ to form Hf. The Hf subsequently reacts with NiTi to form the phase NiTiHf. HfO_2 and $CaHfO_3$ were observed to be the last oxide to reduce, confirming the observations made from the predominance diagram.

(e) The final stage of reduction is the deoxidation and the Ti/Hf homogenisation of NiTiHf alloy. TiC has received much attention as a undesirable phase that is inevitably produced via FFC Cambridge Process. However, this phase was not observed indicating that NiTiHf is resistant to carbide formation.

Acknowledgments

The authors thank John Pillier, Dezhi Li and Martin Davis at the University of Warwick for sharing their expertise during this investigation. The authors thank Luke Marshall, Azeem Mohammed and David Dye at Imperial College London for their help in oxygen analysis and DSC testing. We also thank the China Scholarship Council for providing a scholarship and the Warwick Manufacturing Group for providing funding to enable this research.

References

[1] C. C. Wojcik, *JMEPEG*, 511, 18 (2009).

[2] W. J. Buehler and F. E. Wang, *Ocean Eng.*, 105, 1(1967).

[3] B. K. Jackson, Ph. D. Thesis, University of London (2009).

[4] B. Kockar, I. Karaman, J.I. Kim and Y. Chumlyakov, *Scripta Materialia,* 2203, 54 (2006).

[5] M. Zarinejad, Y. Liu and T. J. White, 876, *Intermetallics*, 16 (2008).

[6] D. Goldverg, Y. Xu, Y. Murakami, S. Otsuka, T. Ueki and H. Horikawa, *Scripta Metall. Mater.*, 1349, 30 (1994).

[7] David S. Grummon, JOM, 24, December 2003.

[8] X. Meng ,Y. Zheng, W. Cai, and L. Zhao, Journal of Alloys and Compounds, 180, 372(2004).

[9] S. F. Hsieh and S. K. Wu, *Journal of Alloys and Compounds*, 237, 270 (1998).

[10] G. Z. Chen, D. J. Fray and T. W. Farthing, *Nature*, 361, 407 (2000).

[11] M. Ma, D. Wang, X. Hu, X, Jin and G. Z. Chen, *Chem. Eur. J.*, 5075, 12 (2006).

[12] Y, Zhu, M. Ma, D, Wang, K Jiang, X. Hu, X. Jin and G. Z. Chen, *Chinese Science Bulletin*, 2535, 51 (2006).

[13] K. Dring , R. Bhagat, M. Jackson, R. Dashwood and D. Inman*, Journal of Alloys and Compounds,* 103, 419 (2006).

[14] R. Bhagat, M. Jackson, D. Inman, and R. Dashwood, *J. Electrochem. Soc.*, E63, 155(2008).

[15] K. Ding, R. Dashwood and D. Inman, *J. Electrochem. Soc.*, D184, 152(2005).

[16] R. Ruh, G. W. Hollenberg, E.G. Charles and V.A. Patel. J. Am. *Ceram. Soc*., 495, 59 (1976).

[17] M. A. Krebs and R. A. Condrate, *Journal of Materials Science Letters*, 1327, 7 (1988).

[18] C. Schwandt and D.J. Fray, *Electrochimica Acta*, 66, 51 (2005).

[19] R. Bhagat, D. Dye, S.L. Raghunathan, R.J. Talling, D. Inman, B. K. Jackson, K. K . Rao and R. J. Dashwood, *Acta Materialia*, 5057, 58 (2010).

[20] B. Jackson, M. Jackson, D. Dye, D. Inman and R. Dashwood, *J. Electrochem. Soc.*, E171, 155(2008).

[21] W Li, X. B. Jin, F. L. Huang and G. Z. Chen, *Angew. Chem. Int. Ed.*, 3203, 49(2010).

[22] W. Xiao, X. B. Jin, Y. Deng, D. H. Wang and G. Z. Chen, *Chem. Eur . J.*, 604, 13(2007).

List of Tables

Table 1

Electrolysis Duration(h)	Phases Present
0(before electrolysis)	$TiNiO_3$, NiO, HfO_2, TiO_2
1/6	Ni, $CaTiO_3$, $Ca(Ti,Hf)O_3$, HfO_2
1	Edge: NiTiHf
	Core: Ni, Ni_3Ti,$CaTiO_3$, $Ca(Ti,Hf)O_3$, HfO_2
3	Edge: NiTiHf
	Core: Ni_3Ti, $CaTiO_3$, $Ca(Ti,Hf)O_3$, HfO_2
5	Edge: NiTiHf
	Core: Ni_3Ti, NiTi, $Ca(Ti,Hf)_2O_4$, $Ca(Ti,Hf)O_3$, HfO_2
9	NiTiHf
17	NiTiHf
24	NiTiHf

Table 2

	A_s, °C	A_f, °C	M_f, °C	M_s, °C
Ni-35Ti-15Hf in this work	190	238	120	168
$Ti_{36}Ni_{49}Hf_{15}$ by Meng *et al.* [8]	216	231	148	179

List of figures

Fig. 11 DSC test result for the 24 h reduced product. The curve on top is during heating and the one below is during cooling.

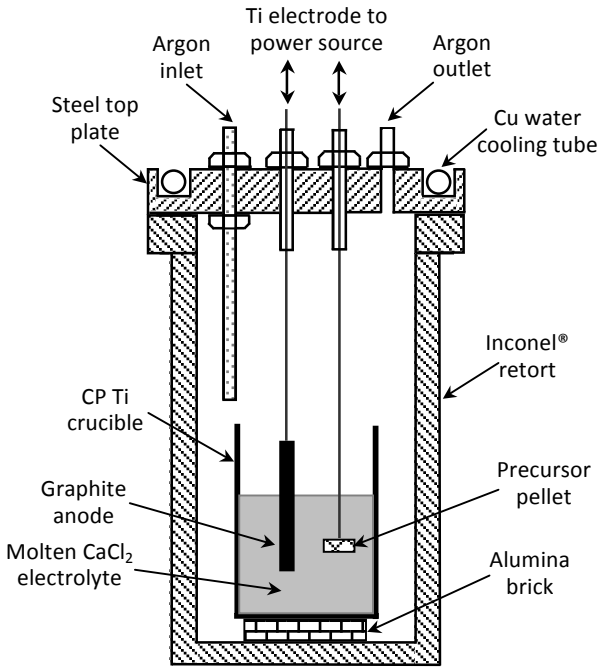

Figure 1

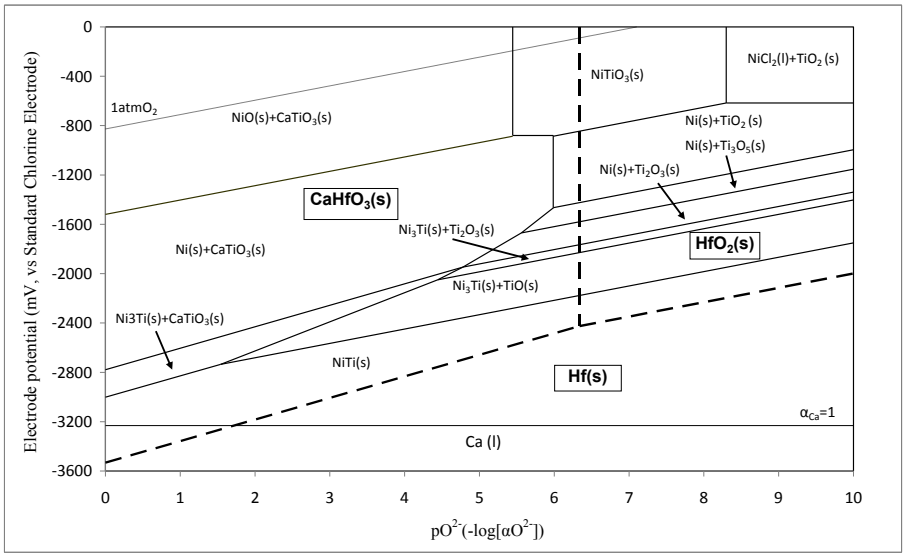
Electrode potential (mV, vs Standard Chlorine Electrode)
0
-400
-800
-1200
-1600
-2000
-2400
-2800
-3200
-3600
0
1
2
3
4
5
6
7
8
9
10
pO2-(-log[αO2-])
1atmO2
NiO(s)+CaTiO3(s)
NiTiO3(s)
NiCl2(l)+TiO2 (s)
Ni(s)+TiO2 (s)
Ni(s)+Ti3O5(s)
Ni(s)+Ti2O3(s)
CaHfO3(s)
Ni3Ti(s)+Ti2O3(s)
Ni(s)+CaTiO3(s)
HfO2(s)
Ni3Ti(s)+TiO(s)
Ni3Ti(s)+CaTiO3(s)
NiTi(s)
Hf(s)
αCa=1
Ca (l)

Figure 2

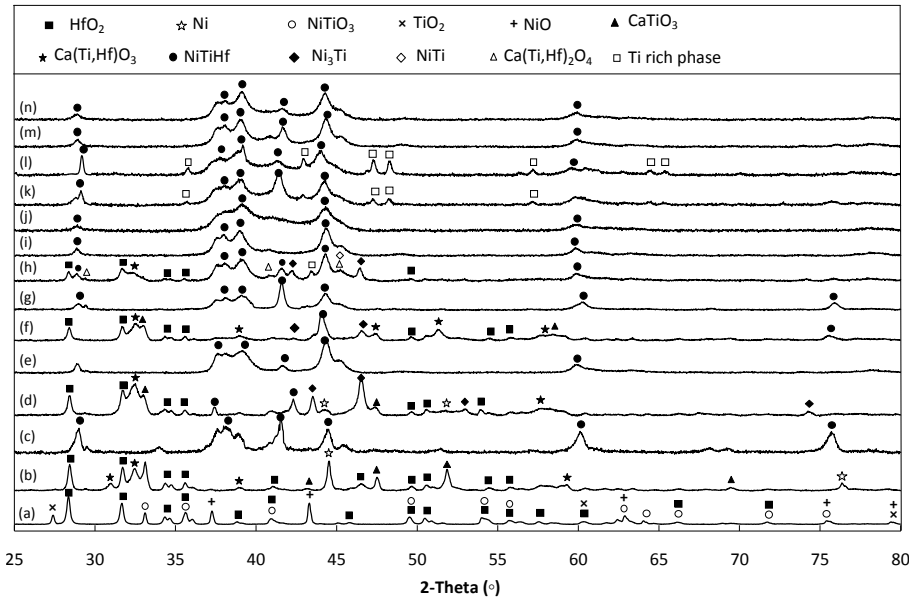
■ HfO2
☆ Ni
○ NiTiO3
× TiO2
+ NiO
▲ CaTiO3
★ Ca(Ti,Hf)O3
● NiTiHf
◆ Ni3Ti
◇ NiTi
▵ Ca(Ti,Hf)2O4
□ Ti rich phase
(n)
(m)
(l)
(k)
(j)
(i)
(h)
(g)
(f)
(e)
(d)
(c)
(b)
(a)
25
30
35
40
45
50
55
60
65
70
75
80
2-Theta (◦)

Figure 3

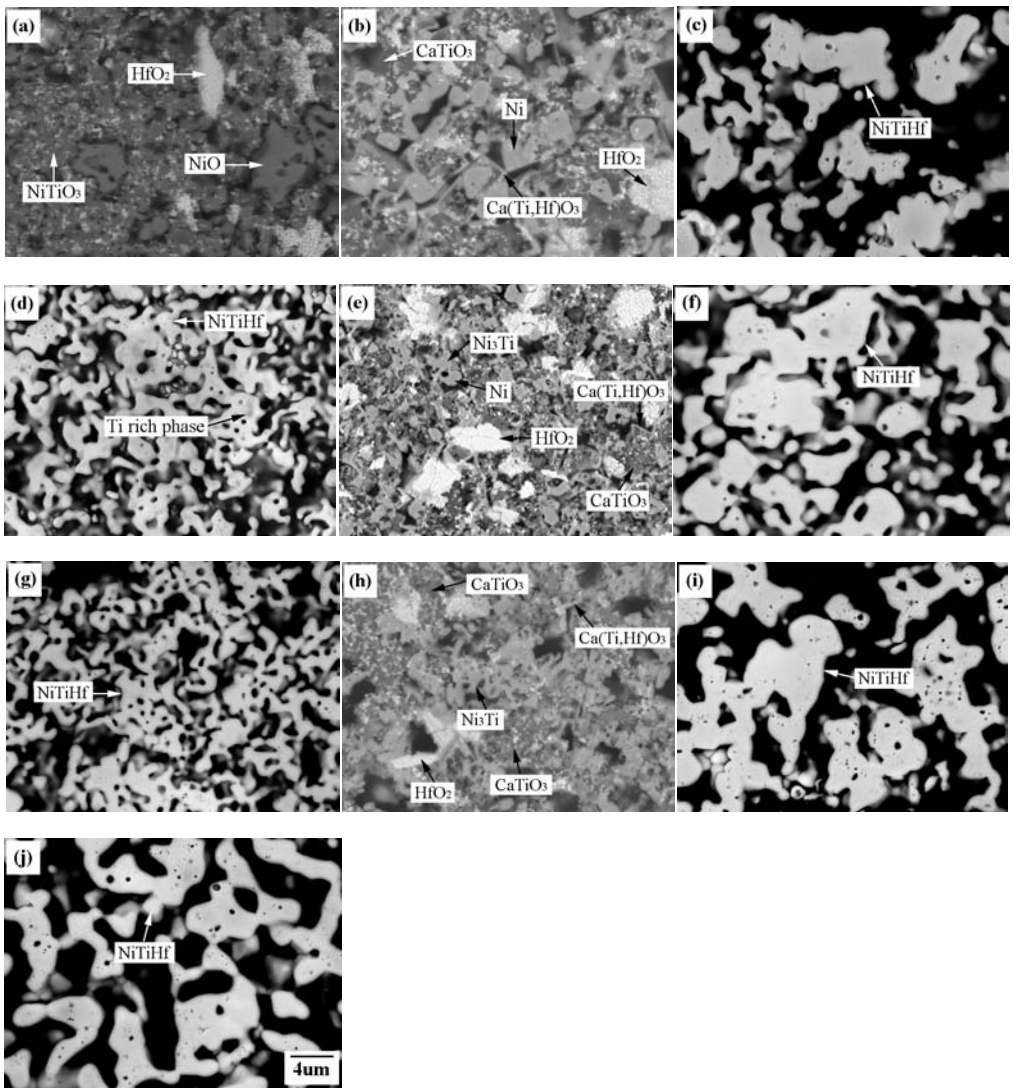
(a)
HfO2
NiO
NiTiO3
(b)
CaTiO3
Ni
HfO2
Ca(Ti,Hf)O3
(c)
NiTiHf
(d)
NiTiHf
Ti rich phase
(e)
Ni3Ti
Ni
Ca(Ti,Hf)O3
HfO2
CaTiO3
(f)
NiTiHf
(g)
NiTiHf
(h)
CaTiO3
Ca(Ti,Hf)O3
Ni3Ti
HfO2
CaTiO3
(i)
NiTiHf
(j)
NiTiHf
4um

Figure 4

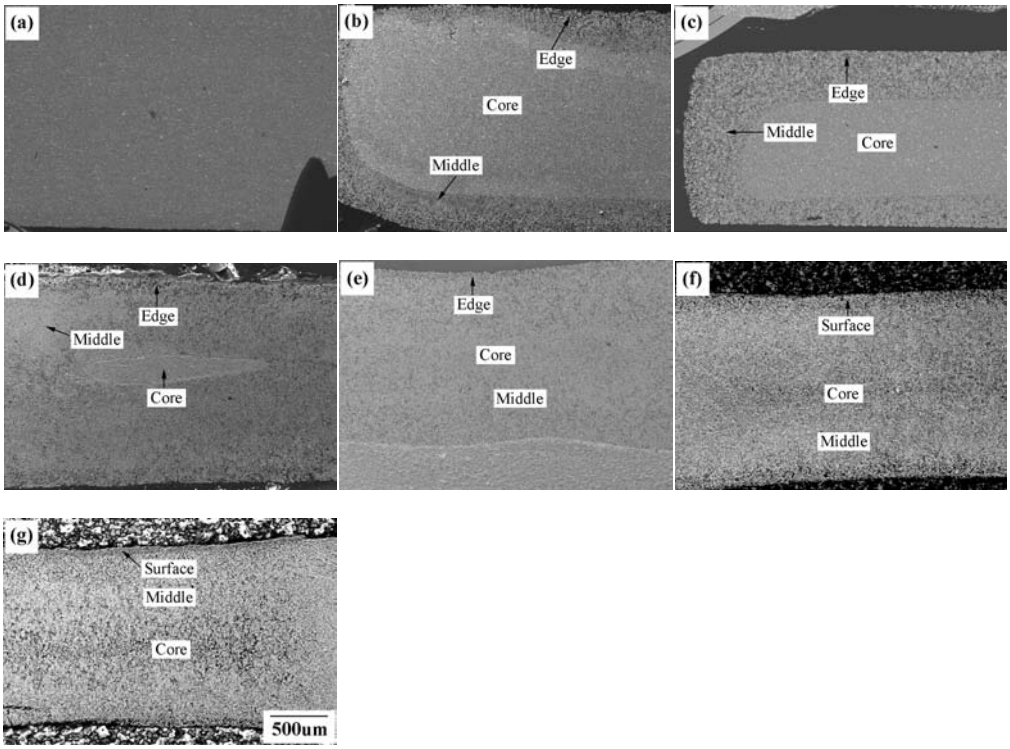
(a)
(b)
Edge
Core
Middle
(c)
Edge
Middle
Core
(d)
Edge
Middle
Core
(e)
Edge
Core
Middle
(f)
Surface
Core
Middle
(g)
Surface
Middle
Core
500um

Figure 5

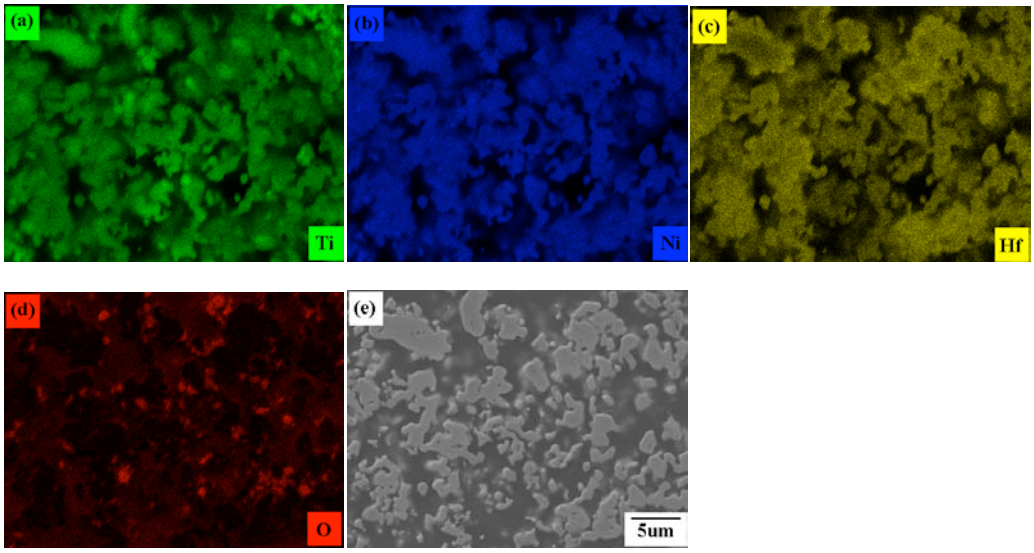

Figure 6

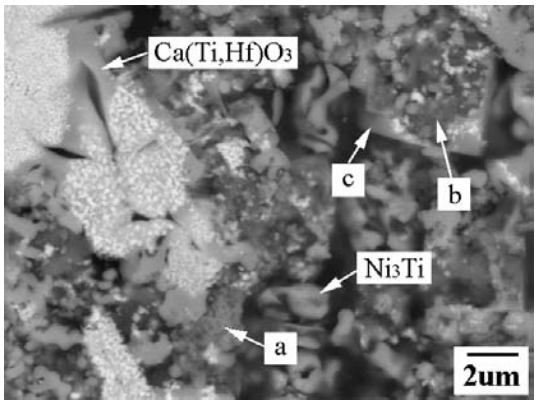

Figure 7

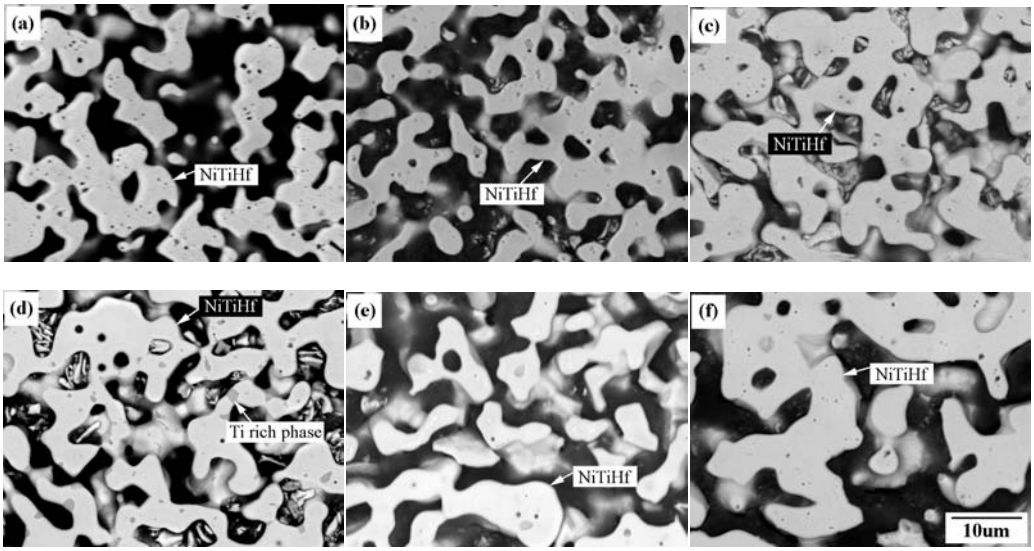
(a)
NiTiHf
(b)
NiTiHf
(c)
NiTiHf
(d)
NiTiHf
Ti rich phase
(e)
NiTiHf
(f)
NiTiHf
10um

Figure 8

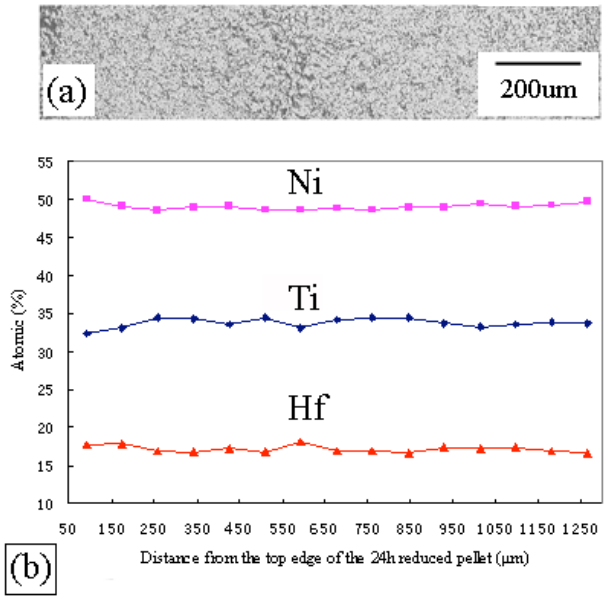
(a)
200um
Ni
Ti
Hf
Atomic (%)
55
50
45
40
35
30
25
20
15
10
50 150 250 350 450 550 650 750 850 950 1050 1150 1250
Distance from the top edge of the 24h reduced pellet (μm)
(b)

Figure 9

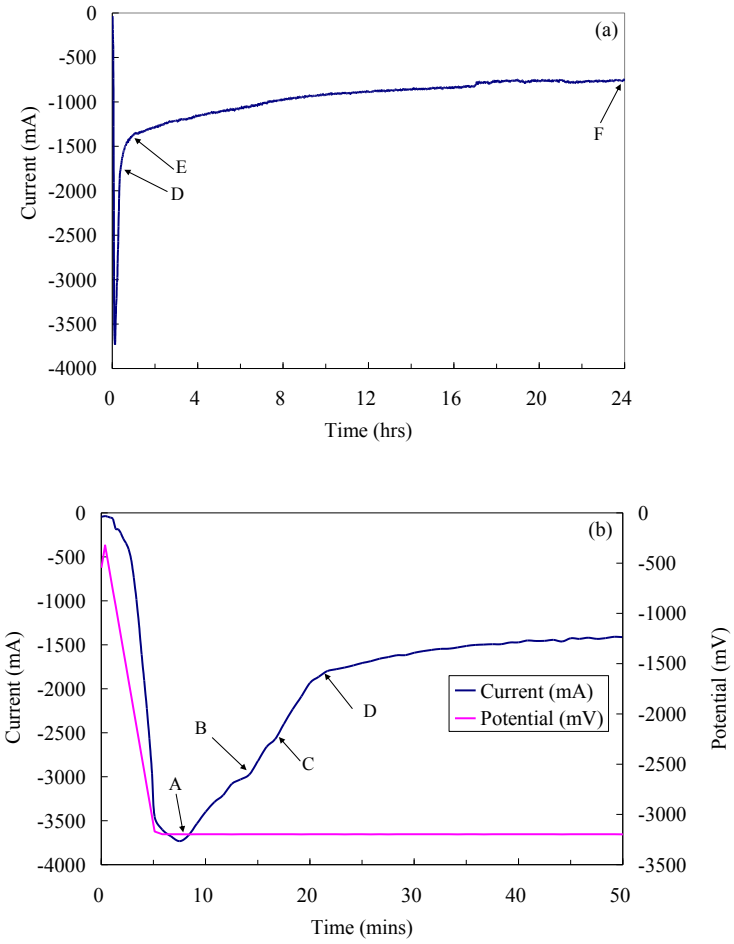
(a)
Current (mA)
Time (hrs)
E
D
F
(b)
Current (mA)
Potential (mV)
Time (mins)
A
B
C
D
Current (mA)
Potential (mV)

Figure 10

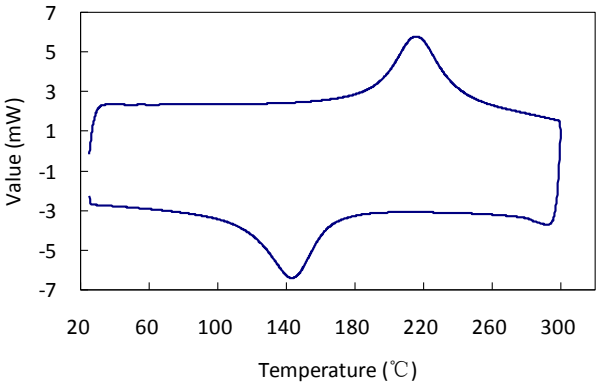

Figure 11